

## Evolutionary Origin of Ultra-long Period Radio Transients

YUN-NING FAN,<sup>1</sup> KUN XU,<sup>1</sup> AND WEN-CONG CHEN<sup>1,2</sup>

<sup>1</sup>*School of Science, Qingdao University of Technology, Qingdao 266525, People's Republic of China; chenwc@pku.edu.cn*

<sup>2</sup>*School of Physics and Electrical Information, Shangqiu Normal University, Shangqiu 476000, People's Republic of China*

### ABSTRACT

Recently, it discovered two ultra-long period radio transients GLEAM-X J162759.5-523504.3 (J1627) and GPM J1839–10 (J1839) with spin periods longer than 1000 s. The origin of these two ultra-long period radio transients is intriguing in understanding the spin evolution of neutron stars (NSs). In this work, we diagnose whether the interaction between strong magnetized NSs and fallback disks can spin NSs down to the observed ultra-long period. Our simulations found that the magnetar+fallback disk model can account for the observed period, period derivative, and X-ray luminosity of J1627 in the quasi-spin-equilibrium stage. To evolve to the current state of J1627, the initial mass-accretion rate of the fallback disk and the magnetic field of the NS are in the range of  $(1.1 - 30) \times 10^{24} \text{ g s}^{-1}$  and  $(2 - 5) \times 10^{14} \text{ G}$ , respectively. In an active lifetime of fallback disk, J1839 is impossible to achieve the observed upper limit of period derivative. Therefore, we propose that J1839 may be in the second ejector phase after the fallback disk becomes inactive. Those NSs with a magnetic field of  $(2 - 6) \times 10^{14} \text{ G}$  and a fallback disk with an initial mass-accretion rate of  $\sim 10^{24} - 10^{26} \text{ g s}^{-1}$  are the possible progenitors of J1839.

*Keywords:* Pulsars: Radio pulsars: accretion: fallback disks: magnetars

### 1. INTRODUCTION

Since the first radio pulsar PSR B1919+21 was discovered (Hewish et al. 1968), about 3500 pulsars have been discovered up to now (Manchester et al. 2005). Radio pulsars are generally thought to be rapidly rotating strongly magnetized neutron stars (NSs), in which the radio emission is powered by the rotational kinetic energy via magnetic dipole radiation (Gold 1968). In the spin period ( $P$ ) versus spin-period derivative ( $\dot{P}$ ) diagram, the  $P$  and  $\dot{P}$  of normal radio pulsars are  $\sim 1 \text{ s}$  and  $\sim 10^{-15} \text{ s s}^{-1}$  (Tauris & van den Heuvel 2006), respectively. As a special population of NSs, the magnetars possess strong magnetic fields ( $\sim 10^{14} \text{ G}$ ) and long spin periods in the range of  $2 - 12 \text{ s}$  (Olausen & Kaspi 2014). The historical lack of radio pulsars with periods longer than  $12 \text{ s}$  was interpreted to be the existence of the "death line", under which the voltage generated above the polar cap is below a critical value (Ruderman & Sutherland 1975; Bhattacharya & van den Heuvel 1991; Chen & Ruderman 1993).

The discovery of some long-period pulsars challenges the conventional pulsar death line model. PSR J0250+5854 (J0250) is a radio pulsar with a spin period of  $23.5 \text{ s}$ , which is in the conventional pulsar death line

(Tan et al. 2018). The Galactic Plane Pulsar Snapshot survey also discovered a long-period pulsar PSR J1903+0433g with a spin period of  $14.05 \text{ s}$  (Han et al. 2021). The discovery of GLEAM-X J162759.5-523504.3 (hereafter J1627) has excited the pulsar community and marked the start of a new era of ultra-long period pulsar field. Hurley-Walker et al. (2022) detected a periodic, low-frequency radio transient J1627, which pulses every 18.18 minutes (1091s). This unusual periodicity challenges our knowledge of the radiation mechanism of pulsars. Subsequently, the discovery of PSR J0901-4046 (J0901) with a spin period of  $75.88 \text{ s}$  supplied a new member for the long-period pulsar population (Caleb et al. 2022). Recently, the discovery of an ultra-long period radio transient GPM J1839–10 (hereafter J1839) is icing on the cake in this population. J1839 was detected to be repeating at a pulsation period of  $1318 \text{ s}$  since at least 1988, and its period derivative is constrained to be less than  $3.6 \times 10^{-13} \text{ s s}^{-1}$  (Hurley-Walker et al. 2023).

It is weird that the radio luminosity ( $4 \times 10^{31} \text{ erg s}^{-1}$ ) inferred from the brightest pulses of J1627 is much higher than its maximum spin-down power ( $\dot{E} = 1.2 \times 10^{28} \text{ erg s}^{-1}$ , Hurley-Walker et al. 2022). Therefore, Hurley-Walker et al. (2022) proposed that J1627 is a radio magnetar rather than a pulsar according to

the properties including the smooth variations in pulse profile and the transient window of radio emission (Levin et al. 2012). Nevertheless, the analysis based on the spectral data suggested that the highest possible radio luminosity of J1627 does not exceed its spin-down luminosity (Erkut 2022). Because of long spin periods, long-period pulsars were proposed to be most likely white dwarfs (Katz 2022) or hot subdwarfs (proto white dwarf, Loeb & Maoz 2022). However, Beniamini et al. (2023) demonstrated that the observations of J1627 are unlikely to be explained by either a magnetically or a rotationally powered white dwarf. Kou et al. (2019) proposed that the long period of J0250 is related to the magnetospheric evolution and magnetic field decay. Ronchi et al. (2022) showed that the newly born NSs with strong magnetic fields of  $10^{14} - 10^{15}$  G and fallback disks with initial accretion rates of  $10^{22} - 10^{27}$  g s $^{-1}$  could evolve into long-period isolated radio pulsars like J1627 and J0901 in a short timescale of  $10^3 - 10^5$  yr.

The first candidate of long-period magnetars is the NS 1E 161348–5055 in the supernova remnant RCW 103, which has an incredibly long period of 6.67 hours (De Luca et al. 2006). Many features of this NS are similar to those of traditional magnetars such as anomalous X-ray pulsars and soft gamma-ray repeaters, including a magnetar-like short X-ray burst (D’Ài et al. 2016), longer-term outbursts, and a hard X-ray tail in the spectrum during outburst (Rea et al. 2016). The NS should be a young magnetar because the age of RCW 103 was inferred to be  $\sim 3.3$  kyr (Clark & Caswell 1976) or in the range of 1.2 – 3.2 kyr (Nugent et al. 1984; Carter et al. 1997). Recently, detailed modeling of the supernova remnant estimated the age of the source to be 880 – 4400 yr (Braun et al. 2019). The emission properties also imply that 1E 161348–5055 should be a young magnetar, in which the 6.67 hr periodicity can only be thought to be the spin period of the magnetar (Rea et al. 2016). It is extremely anomalous that the spin period of this source is much longer than those (2 – 12 s) of traditional magnetars. Ignored the ejector phase, De Luca et al. (2006) found that a magnetic field of  $B = 5 \times 10^{15}$  G and a debris disc mass of  $3 \times 10^{-5} M_{\odot}$  can spin the NS down to the present period in propeller phase. Subsequent some detailed simulation also confirmed the magnetar nature of 1E 161348–5055 (Li 2007; De Luca et al. 2008; Esposito et al. 2011; D’Ài et al. 2016; Rea et al. 2016; Tong et al. 2016; Ho & Andersson 2017; Tendulkar et al. 2017; Borghese et al. 2018; Xu & Li 2019). Beniamini et al. (2020) demonstrated that an episodic mass-loaded charged particle winds can efficiently spin a magnetar down to an ultra-long period.

Compared with 1E 161348–5055, J1627 and J1839 were detected the upper limit of period derivative as  $\dot{P} = 1.2 \times 10^{-9}$  s s $^{-1}$  (Hurley-Walker et al. 2022) and  $\dot{P} = 3.6 \times 10^{-13}$  s s $^{-1}$  (Hurley-Walker et al. 2023), respectively. Especially, J1839 is located at the very edge of an extremely tolerant death line, making it impossible as a classical radio pulsar (Hurley-Walker et al. 2023). However, Tong (2023a) suggested that the pulsar death line of long-period pulsars should be revised due to two possible physical effects of a fallback disk or a twisted magnetic field, and J1627 may be a radio-loud magnetar spun down by a fallback disk. Recently, J1627 and J1839 were thought to be most likely magnetars with twisted magnetic fields, magnetars with fallback disk, or white dwarf radio pulsars (Tong 2023b). Therefore, the possibility that J1839 is a radio magnetar cannot be completely excluded.

In this work, we attempt to diagnose whether the magnetar + fallback disk model can account for the long spin periods and period derivative of ultra-long period radio transients J1627 and J1839. Meanwhile, we also investigate the initial parameter space producing these two transients. In Section 2, we describe the detailed physical model including fallback disk, ejector phase, and propeller phases. The simulated results of the sources J1627 and J1839 are summarized in Section 3. Finally, we give a brief discussion and summary in Sections 4 and 5.

## 2. PHYSICAL MODEL

### 2.1. *Fallback disk*

Isolated NSs are the evolutionary products of massive stars through core-collapse supernovae when their progenitors exhaust all fuels. During supernovae explosions, a tiny fraction of ejecta could form a fallback disk surrounding the nascent NS rather than completely leave it because those ejecta possess a sufficient angular momentum (Michel 1988; Lin et al. 1991; Perna et al. 2014). Two normal magnetars 4U 0142+61 and 1E 2259+586 are most likely to be surrounded by fallback disks (Wang et al. 2006; Kaplan et al. 2009). Without the interaction between the fallback disk and the NS, the spin evolution of the NS is driven by magnetic dipole radiation and is in an ejector phase in the early stage. With the increase of the spin period, the fallback disk can interact with the NS magnetosphere, and the NS enters a propeller phase. In this phase, a propeller torque originated from the interaction between the fallback disk and the NS can significantly influence the spin evolution of the NS (Illarionov & Sunyaev 1975), and the spin angular velocity of the NS decreases at an ex-

ponential rate for a short time  $t_{\text{prop}}$  (see also Eq. 13, Ho & Andersson 2017).

In the most lifetime, the accretion rate in the fallback disk decreases self-similarly according to a power-law as  $\dot{M} \propto t^{-\alpha}$  ( $t$  is the age of the fallback disk), in which  $\alpha = 19/16$  for a fallback disk whose opacity is dominated by electron scattering (Cannizzo et al. 1990). In the calculation, we adopt an accretion rate whose evolutionary law same to Chatterjee et al. (2000) as follows

$$\dot{M} = \begin{cases} \dot{M}_0, & t < T \\ \dot{M}_0(t/T)^{-\alpha}, & t \geq T \end{cases} \quad (1)$$

where  $\dot{M}_0$  is the initial mass-accretion rate when  $t < T$ , in which  $T$  is of the order of the dynamical timescale in the inner region of the nascent fallback disk. Chatterjee et al. (2000) adopted a typical value of  $T = 1$  ms. Similar to Menou et al. (2001), we take  $T = 2000$  s (Tong et al. 2016; Ronchi et al. 2022), which can be derived from a typical viscous timescale that the fallback material with excess angular momentum circularizes to form a disk. Since  $T = 6.6 \times 10^{-5}$  yr is much smaller than the age ( $10^3 - 10^4$  yr) of long-period pulsars, the accretion process in the early stage ( $t < T$ ) is negligible in our simulations. Since the initial mass of the fallback disk satisfies

$$M_{\text{d,i}} = \dot{M}_0 T + \int_T^\infty \dot{M}_0(t/T)^{-\alpha} dt, \quad (2)$$

we have  $\dot{M}_0 = (\alpha - 1)M_{\text{d,i}}/(\alpha T)$  (Chen 2022).

In general, the inner radius of the fallback disk is thought to be the magnetospheric radius, at which the magnetic energy density is equal to the kinetic energy density of the inflow material. The magnetospheric radius is given by (Davidson & Ostriker 1973; Elsner & Lamb 1977; Ghosh & Lamb 1979)

$$R_{\text{m}} = \xi \left( \frac{\mu^4}{2GM\dot{M}^2} \right)^{1/7} = 7.5 \times 10^8 \text{ cm } \xi_{0.5} \quad (3)$$

$$\times M_{1.4}^{-1/7} B_{14}^{4/7} R_6^{12/7} \dot{M}_{18}^{-2/7},$$

where  $G$  is the gravitational constant,  $M$  is the NS mass,  $\dot{M}$  is the accretion rate,  $\mu = BR^3/2$  ( $B$  and  $R$  are the surface magnetic field and the radius of the NS) is the magnetic dipole moment of the NS, and  $\xi \approx 0.5$  is a corrective factor (Wang 1996; Long et al. 2005). In equation 3,  $M_{1.4} = M/1.4 M_\odot$ ,  $R_6 = R/10^6$  cm,  $B_{14} = B/10^{14}$  G, and  $\dot{M}_{18} = \dot{M}/10^{18}$  g s $^{-1}$ .

## 2.2. Ejector phase

In the early stage after the NS was born, the inner radius of the fallback disk is greater than the light-cylinder

radius, which is defined as

$$R_{\text{lc}} = Pc/2\pi = 4.8 \times 10^6 \text{ cm } P_{-3}, \quad (4)$$

where  $c$  is the speed of light in vacuo,  $P_{-3} = P/10^{-3}$  s is the spin period of the NS. In this stage, the rapidly rotating NS cannot interact with the accreted material, appearing as a radio pulsar, that is the ejector phase. The NS could radiate strong radio emission by the magnetic dipole radiation, which exerts a braking torque on the NS as follows

$$N_{\text{md}} = -\frac{2\mu^2\Omega^3 \sin^2\theta}{3c^3} = -\beta I\Omega^3, \quad (5)$$

where  $\Omega = 2\pi/P$  is spin angular velocity of the NS,  $\theta$  is the inclination angle between the magnetic axis and the rotation axis,  $I$  is the momentum of inertia. For simplicity, in this work we assume an orthogonal rotator, i.e.  $\theta = \pi/2$ , thus  $\beta \equiv 2\mu^2/3c^3I$ . According to the law of rotation  $N_{\text{md}} = I\dot{\Omega}$ , we have  $\dot{\Omega} = -\beta\Omega^3$ . Therefore, in the ejector phase, the spin period of the NS satisfies

$$P = P_0 \left( 1 + \frac{8\beta\pi^2 t}{P_0^2} \right)^{1/2} = P_0 \left( 1 + \frac{t}{t_{\text{em}}} \right)^{1/2}, \quad (6)$$

where  $P_0$  is the initial spin period of the NS. Due to magnetic dipole radiation, the nascent NS spin down on the timescale

$$t_{\text{em}} = \frac{P_0}{2\dot{P}_0} = \frac{P_0^2}{8\pi^2\beta} = 2.1 \times 10^5 \text{ s } \frac{P_{0,-3}^2 I_{45}}{B_{14}^2 R_6^6}, \quad (7)$$

where  $I_{45} = I/10^{45}$  g cm $^2$ .

With the spin-down of the NS, the light-cylinder radius gradually increases. Once  $R_{\text{m}} < R_{\text{lc}}$ , the NS magnetosphere can interact with the fallback disk, and the propeller phase begins. The transition period (i.e. the maximum period of the ejector phase) between the ejector phase and the propeller phase is

$$P_{\text{ej,max}} = \frac{2\pi}{\Omega_{\text{ej,max}}} = \frac{2\pi R_{\text{m}}}{c} = 0.16 \text{ s } \xi_{0.5} \quad (8)$$

$$\times M_{1.4}^{-1/7} B_{14}^{4/7} R_6^{12/7} \dot{M}_{18}^{-2/7}.$$

Inserting Equation (8) into Equation (6), we can estimate the duration of the ejector phase to be

$$t_{\text{ej}} = t_{\text{em}} \left[ \left( \frac{P_{\text{ej,max}}}{P_0} \right)^2 - 1 \right] \approx 164 \text{ yr } \xi_{0.5}^2 \quad (9)$$

$$\times M_{1.4}^{-2/7} R_6^{-18/7} I_{45} B_{14}^{-6/7} \dot{M}_{18}^{-4/7}.$$

In Equation (9),  $\dot{M}$  is time-varying, while  $t_{\text{ej}}$  should be a constant. According to  $\dot{M}_{18} = \dot{M}_{0,18}(t/T)^{-19/16}$ ,  $t = t_{\text{ej}}$ , and Equation (8), it yields

$$t_{\text{ej}} = \left( 164 \text{ yr } \xi_{0.5}^2 M_{1.4}^{-\frac{2}{7}} R_6^{-\frac{18}{7}} I_{45} B_{14}^{-\frac{6}{7}} \dot{M}_{0,18}^{-\frac{4}{7}} T^{-\frac{19}{28}} \right)^{\frac{28}{9}}, \quad (10)$$

where  $T$  in units of second.

### 2.3. Propeller phase

The NS enters the propeller phase once the inner radius of the fallback disk is located between the light-cylinder radius and the corotation radius, in which the corotation radius is defined as

$$R_{\text{co}} = \sqrt[3]{\frac{GM P^2}{4\pi^2}} = 1.7 \times 10^6 \text{ cm } M_{1.4}^{1/3} P_{-3}^{2/3}. \quad (11)$$

During the propeller phase ( $R_c \leq R_m \leq R_{\text{lc}}$ ), the Keplerian angular velocity ( $\Omega_K(R_m) = \sqrt{GM/R_m^3}$ ) at the magnetosphere radius of the fallback disk is smaller than the spin angular velocity of the NS. Therefore, the accreted material cannot keep co-rotating with the NS and was thought to be ejected at  $R_m$  due to the centrifugal barrier, resulting in a negative torque exerted on the NS. Meanwhile, the interaction between the magnetic lines and the fallback disk also produces a similar negative torque (Menou et al. 1999). The detailed numerical simulations indicate that the two braking torques mentioned above is approximately equal (Daumerie 1996). As a consequence, a braking torque exerting on the NS in the propeller phase can be expressed as

$$N_{\text{prop}} = 2\dot{M}R_m^2(\Omega_K(R_m) - \Omega), \quad (12)$$

where the factor of 2 originates from the two nearly equal negative torques mentioned above. Our adopted braking torque is two times as large as that taken by Ho & Andersson (2017), in which the interaction between the magnetic field lines and the fallback disk is ignored.

According to the law of rotation, the time derivative of the NS spin can be calculated from

$$\dot{\Omega} = -\frac{2\dot{M}R_m^2}{I}(\Omega - \Omega_K(R_m)) = -\frac{\Omega - \Omega_K(R_m)}{t_{\text{prop}}}, \quad (13)$$

where

$$t_{\text{prop}} = 28.2 \text{ yr } I_{45} \xi_{0.5}^{-2} M_{1.4}^{2/7} B_{14}^{-8/7} R_6^{-24/7} \dot{M}_{18}^{-3/7}. \quad (14)$$

It is worth noting that  $t_{\text{prop}}$  changes with time in our model, which is different with the model of Ho & Andersson (2017). Therefore, we have to use a numerical method to calculate the spin evolution of the NS in the propeller phase.

## 3. EVOLUTIONARY MODELS OF ULTRA-LONG PERIOD RADIO TRANSIENTS

### 3.1. Initial values and input parameters

In the ejector phase, we use Equation (6) to calculate the spin evolution of the NS. Once the NS transitions to the propeller phase, we adopt a numerical method

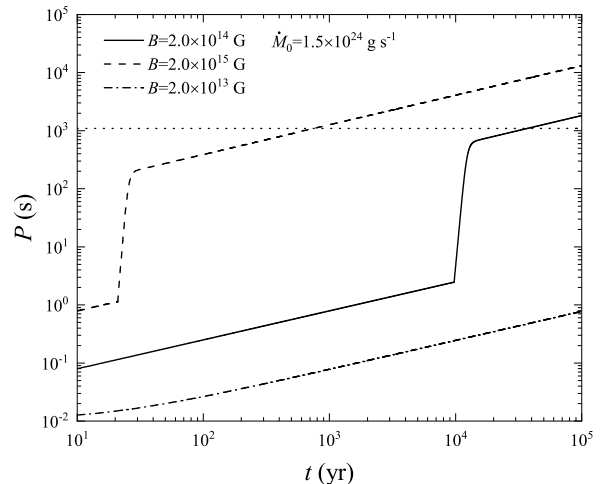


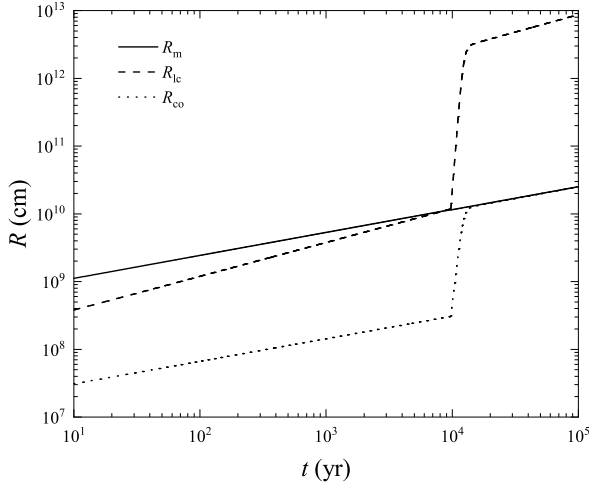
**Figure 1.** Evolution of spin periods of NSs surrounding a fallback disk with an initial mass-accretion rate  $\dot{M}_0 = 1.5 \times 10^{24} \text{ g s}^{-1}$  for different surface magnetic fields. The solid, dashed, and dashed-dotted curves denote the evolutionary tracks of NSs with  $B = 2.0 \times 10^{14}$ ,  $2.0 \times 10^{15}$ , and  $2.0 \times 10^{13}$  G, respectively. The horizontal dotted line represents the present period  $P = 1091$  s of radio transient J1627.

based on Equations (13) and (14) to simulate its spin evolution. For simplicity, we take  $\xi_{0.5} = M_{1.4} = R_6 = I_{45} = 1$ . The spin period of the nascent NS is thought to be  $P_0 = 10$  ms ( $P_{0,-3} = 10$ ). Adopting the above input parameters, the spin evolution of the NS is governed by two input parameters including its magnetic field  $B$  and the initial mass-accretion rate  $\dot{M}_0$  of the fallback disk.

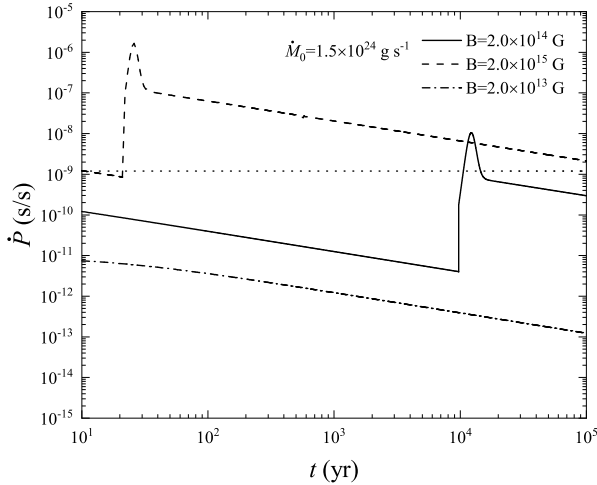
### 3.2. Radio transient J1627

Figure 1 shows the evolutionary tracks of NSs with an initial mass-accretion rate  $\dot{M}_0 = 1.5 \times 10^{24} \text{ g s}^{-1}$  and different surface magnetic fields in the spin period versus NS age diagram. In the ejector phase, the spin periods evolve along lines with the same slope of  $\Delta \log(P/\text{s}) / \Delta \log(t/\text{yr}) = 1/2$ . This law arises from a simple relation  $P \approx P_0(t/t_{\text{em}})^{1/2}$  when  $t/t_{\text{em}} \gg 1$  according to Equation (6). The final period in the ejector phase is  $P_{\text{ej,max}}$ , and the duration of the ejector phase  $t_{\text{ej}} \propto B_{14}^{-8/3}$  for a fixed  $\dot{M}_0$ . Therefore, a strong magnetic field naturally results in a short duration of the ejector phase like in Figure 1. In contrast, the NS with a weak magnetic field of  $2.0 \times 10^{13}$  G is always in the ejector phase in a timescale of  $10^5$  yr, and merely evolves to a period of 0.8 s. Furthermore, from Equations (2), (8), and (10), we can derive the evolutionary law of  $P_{\text{ej,max}}$  as

$$P_{\text{ej,max}} \propto B_{14}^{4/7} t_{\text{ej}}^{19/56} \propto B_{14}^{-1/3}. \quad (15)$$



**Figure 2.** Evolution of the three critical radii of an NS with a fallback disk of an initial mass-accretion rate  $\dot{M}_0 = 1.5 \times 10^{24} \text{ g s}^{-1}$  and a surface magnetic field  $B = 2.0 \times 10^{14} \text{ G}$ . The solid, dashed, and dotted curves denote the evolutionary tracks of the magnetospheric radius, light-cylinder radius, and co-rotation radius, respectively.



**Figure 3.** Spin-period derivatives of NSs as a function of ages in the existence of a fallback disk with an initial mass-accretion rate  $\dot{M}_0 = 1.5 \times 10^{24} \text{ g s}^{-1}$ . The solid, dashed, and dashed-dotted curves denote the evolutionary tracks of NSs with  $B = 2.0 \times 10^{14}$ ,  $2.0 \times 10^{15}$ , and  $2.0 \times 10^{13} \text{ G}$ , respectively. The horizontal dotted line represents the upper limit ( $\dot{P} = 1.2 \times 10^{-9} \text{ s s}^{-1}$ ) of the period derivative of J1627.

As a consequence, a strong magnetic field produces a short  $P_{\text{ej,max}}$ . After  $P_{\text{ej,max}}$ , the NS transitions to the propeller phase, and its spin period increases at an exponential rate. The two NSs with strong magnetic field  $B = 2.0 \times 10^{15}$  and  $2.0 \times 10^{14} \text{ G}$  can evolve to the present period (1091 s) of J1627 at  $t = 748$  and  $3.7 \times 10^4 \text{ yr}$ , respectively.

The model with an initial mass-accretion rate  $\dot{M}_0 = 1.5 \times 10^{24} \text{ g s}^{-1}$  and a surface magnetic field  $B = 2.0 \times 10^{14} \text{ G}$  can successfully reproduce the observed  $P$  and  $\dot{P}$  of J1627. We depict the evolution of the three critical radii of the NS in Figure 2. During the ejector phase,  $R_m > R_{\text{lc}} > R_{\text{co}}$ , and the NS spins down due to magnetic dipole radiation. At  $t = 9.7 \times 10^3 \text{ yr}$ ,  $R_m = R_{\text{lc}} > R_{\text{co}}$ , and the NS transitions to the propeller phase. Subsequently,  $R_{\text{lc}} > R_m > R_{\text{co}}$ , and the spin period of the NS rapidly increases at an exponential rate due to the propeller torque. With the increase of the spin period, the corotation radius also increases at an exponential rate. When  $R_{\text{co}}$  increases to be approximately equal to  $R_m$ , the NS reaches a quasi-spin equilibrium, and the quasi-equilibrium period is given by

$$P_{\text{eq}} = 9.3 \text{ s } B_{14}^{6/7} \dot{M}_{18}^{-3/7} \propto t^{57/112}. \quad (16)$$

As a consequence, the spin period of the NS slowly increases in the quasi-spin-equilibrium stage. Because the slope of the evolutionary track is  $\Delta \log(P_{\text{eq}}/\text{s}) / \Delta \log(t/\text{yr}) = 57/112 \approx 1/2$ , it seems that the two evolutionary lines of spin periods in the ejector phase and the quasi-spin-equilibrium stage are parallel (see also Figure 1).

Figure 3 plots the evolutionary tracks of NSs with  $\dot{M}_0 = 1.5 \times 10^{24} \text{ g s}^{-1}$  and different surface magnetic fields in the spin-period derivative versus NS age diagram. It is clear that the evolutionary tracks in the ejector phase are lines with the same slope. This phenomenon is caused by the evolutionary law of spin-period derivative. In the ejector phase, the evolution of the period derivative is governed by

$$\dot{P} = \frac{4\pi^2\beta}{P} = \frac{4\pi^2\beta}{P_0} \left(1 + \frac{t}{t_{\text{em}}}\right)^{-1/2}. \quad (17)$$

When  $t/t_{\text{em}} \gg 1$ , Equation (17) can derive to  $\dot{P} \propto (t/t_{\text{em}})^{-1/2}$ , hence the spin-period derivatives evolve along lines with a slope of  $\Delta \log(\dot{P}/\text{s s}^{-1}) / \Delta \log(t/\text{yr}) = -1/2$ . The period derivatives decrease to  $\dot{P} \sim 10^{-12} - 10^{-9} \text{ s s}^{-1}$ , depending on the surface magnetic fields of NSs. A strong surface magnetic field tends to result in a high final period derivative in the ejector phase.

Once the NS transitions to the propeller phase, the spin-period derivatives rapidly climb to a peak, and then

decline. The evolutionary law of the period derivative is

$$\dot{P} = -\frac{2\pi\dot{\Omega}}{\Omega^2}, \quad (18)$$

where  $\dot{\Omega}$  is derived from Equation (13). Therefore, a rapidly decreasing angular velocity produces a quick increasing  $\dot{P}$ . For the NS with  $B = 2.0 \times 10^{14}$  G, our simulated  $\dot{P} = 4.8 \times 10^{-10}$  ss $^{-1}$  at the current age ( $3.7 \times 10^4$  yr) of J1627, which is less than the observed upper limit ( $1.2 \times 10^{-9}$  ss $^{-1}$ ) of period derivative of J1627 (Hurley-Walker et al. 2022). Based on the observed period and period derivative, the characteristic age of J1627 can be constrained to be  $\tau_c = P/(2\dot{P}) > 1.4 \times 10^4$  yr. Our simulated age is compatible with the characteristic age of J1627. The NS with a strong magnetic field of  $B = 2.0 \times 10^{15}$  G can evolve to 1091 s at an age of 748 yr, while the corresponding period derivative is much higher than the observed value. From Equation (16), it can derive  $\dot{P}_{\text{eq}} \propto t^{-55/112}$ , thus, the slope of the evolutionary lines of  $\dot{P}_{\text{eq}}$  is  $\Delta \log(\dot{P}_{\text{eq}})/\Delta \log(t/\text{yr}) = -55/112 \approx -1/2$ . As a consequence, it seems that the two evolutionary lines of period derivatives in the ejector phase and the quasi-spin-equilibrium stage are parallel in Figure 3.

In our best model, the current mass-accretion rate of J1627 is  $\dot{M} = \dot{M}_0(t/2000 \text{ s})^{-19/16} = 5.8 \times 10^{13}$  g s $^{-1}$  when its current age  $t = 3.7 \times 10^4$  yr. Therefore, the current X-ray luminosity of the NS can be calculated by

$$L_X = \frac{GM\delta\dot{M}_c}{R} = 1.0 \times 10^{32} \text{ erg s}^{-1} M_{1.4} R_6^{-1} \left( \frac{\delta}{0.01} \right) \left( \frac{\dot{M}_c}{5.8 \times 10^{13} \text{ g s}^{-1}} \right), \quad (19)$$

where  $\delta$  is the accretion efficiency of the NS in the propeller phase. Since J1627 was observed an upper limit ( $L_X < 1.0 \times 10^{32}$  erg s $^{-1}$ ) of X-ray luminosity (Hurley-Walker et al. 2022), it implies that the accretion efficiency of the NS is smaller than 1% if the observed X-ray luminosity originates from an accretion from the fallback disk. Such an accretion efficiency is slightly lower than the estimated values (0.01–0.05) in the observation and theoretical researches (Cui 1997; Zhang et al. 1998; Papitto & Torres 2015; Tsygankov et al. 2016).

Figure 4 presents the influence of the initial mass-accretion rates of fallback disks on the spin evolution of NSs. Because of the same magnetic field, the spin periods of NSs with different initial mass-accretion rates of fallback disks evolve along the same line in the ejector phase, while their durations are different. From Equation (10), it can derive  $t_{\text{ej}} \propto \dot{M}_0^{-16/9}$ , thus, a

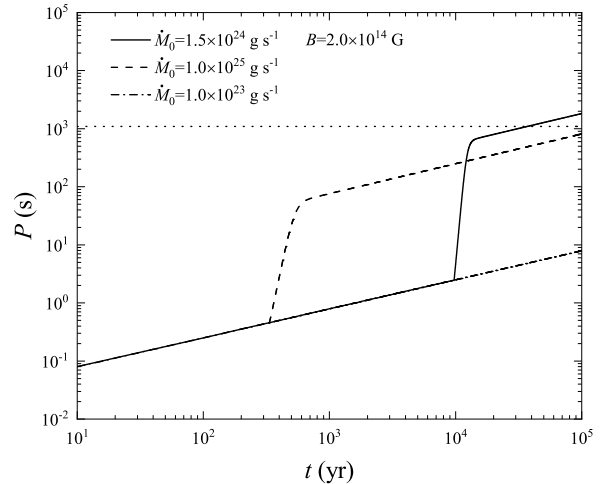


**Figure 4.** Evolution of spin periods of NSs surrounding a fallback disk with different initial mass-accretion rates and a surface magnetic field  $B = 2.0 \times 10^{14}$  G. The solid, dashed, and dashed-dotted curves denote the initial mass-accretion rates of the fallback disks  $\dot{M}_0 = 1.5 \times 10^{24}$ ,  $1.0 \times 10^{25}$ , and  $1.0 \times 10^{23}$  g s $^{-1}$ , respectively. The horizontal dotted line represents the present period  $P = 1091$  s of radio transient J1627.

high initial mass-accretion rate results in a short duration in the ejector phase. After the NSs transition to the propeller phase, they quickly reach a quasi-spin equilibrium. A high initial mass-accretion rate naturally produces a short initial quasi-equilibrium period according to Equation (16). Therefore, the NS with  $\dot{M}_0 = 1.0 \times 10^{25}$  g s $^{-1}$  spends a timescale longer than the NS with  $\dot{M}_0 = 1.5 \times 10^{24}$  g s $^{-1}$  to evolve to the current period of J1627.

Figure 5 summarizes the parameter space that can produce the ultra-long period radio transient J1627 in the magnetic field versus the initial mass-accretion rate diagram. Those magnetars with a magnetic field of  $(2-5) \times 10^{14}$  G and a fallback disk with an initial mass-accretion rate of  $(1.1-30) \times 10^{24}$  g s $^{-1}$  can evolve toward the radio transient J1627 with a spin period of 1091 s, a period derivative less than  $1.2 \times 10^{-9}$  ss $^{-1}$ , and an X-ray luminosity less than  $10^{32}$  erg s $^{-1}$  (taking a relatively low accretion efficiency  $\delta = 0.001$ , we calculate the X-ray luminosity of the NS in the propeller phase according to equation 19) in a timescale shorter than  $10^5$  yr. It is worth emphasizing that the parameter space strongly depends on the accretion efficiency during the propeller phase. The parameter space would sharply reduce to an ultra-small zone in the lower-left shaded area if the accretion efficiency  $\delta = 0.01$ . To form the ultra-long spin period, a strong magnetic field tends to require a high

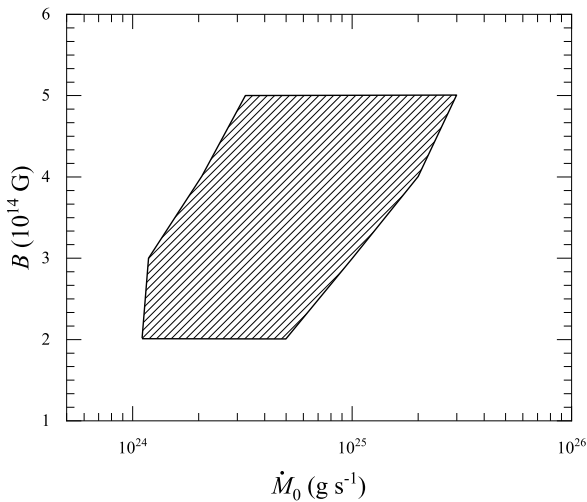


**Figure 5.** Parameter space that can produce the ultra-long period radio transient J1627 in magnetic field vs. initial mass-accretion rate diagram. Those nascent NSs with a magnetic field and an initial mass-accretion rate in the shaded region can evolve into the radio transient J1627 with a spin period of 1091 s, a period derivative less than  $1.2 \times 10^{-9} \text{ s s}^{-1}$ , and an X-ray luminosity less than  $10^{32} \text{ erg s}^{-1}$  in a timescale shorter than  $10^5 \text{ yr}$ .

initial mass-accretion rate. If  $t_{\text{prop}}$  is a constant, it can derive to  $\Omega = [\Omega_{\text{ej,max}} - \Omega_{\text{k}}(R_{\text{m}})]e^{-(t-t_{\text{ej}})/t_{\text{prop}}} + \Omega_{\text{k}}(R_{\text{m}})$  from Equation (13). Therefore,  $t_{\text{prop}}$  is a characteristic timescale that the spin period changes in the propeller phase. A suitable  $t_{\text{prop}}$  will determine whether the NS can evolve to an ultra-long spin period. According to Equation (14), a strong magnetic field naturally requires a high initial mass-accretion rate for a fixed  $t_{\text{prop}}$ . According to Figure 4, a high initial mass-accretion rate can not produce ultra-long period NS in a timescale shorter than  $10^5 \text{ yr}$ , resulting in the right boundary of the shaded region. An NS with a strong magnetic field would evolve toward the state exceeding the upper limits of the observed period derivative and X-ray luminosity, resulting in the upper boundary. Meanwhile, the bottom and left boundaries originate from the lower limits of the magnetic field and initial mass-accretion rate, under which the NS is always in the ejector phase.

### 3.3. Radio transient J1839

#### 3.3.1. J1839 is in the propeller phase

We first consider that J1839 is still in the propeller phase at present. Figure 6 shows the evolutionary trajectories of  $P$  and  $\dot{P}$  of NSs with the initial mass-accretion rate  $\dot{M}_0 = 1.0 \times 10^{25} \text{ g s}^{-1}$  and different magnetic fields. The NS with a weak magnetic field

of  $B = 1.0 \times 10^{12} \text{ G}$  is permanently in the ejector phase in a timescale of  $10^8 \text{ yr}$ , and cannot evolve to an ultra-long period. The two NSs with magnetic fields of  $B = 1.0 \times 10^{14}$  and  $7.9 \times 10^{12} \text{ G}$  can evolve to the current period of J1839 in ages of  $8.3 \times 10^5$  and  $6.0 \times 10^7 \text{ yr}$ , respectively. In the case of  $B = 7.9 \times 10^{12} \text{ G}$ , the current period derivative  $\dot{P} = 3.55 \times 10^{-13} \text{ s s}^{-1}$ . However, the NS with  $B = 1.0 \times 10^{14} \text{ G}$  spends a timescale longer than its current age to evolve to the observed upper limit ( $\dot{P} = 3.6 \times 10^{-13} \text{ s s}^{-1}$ ) of the period derivative.

Similar to J1627, we also investigate whether it can produce the observed properties of J1839 in a wide range of magnetic fields and initial mass-accretion rates. Those NSs with initial mass-accretion rates of  $\dot{M}_0 = 10^{23} - 10^{30} \text{ g s}^{-1}$  and magnetic fields of  $B = 10^9 - 10^{16} \text{ G}$  cannot evolve to the current period and period derivative ( $\dot{P} < 3.6 \times 10^{-13} \text{ s s}^{-1}$ ) in a timescale shorter than  $10^7 \text{ yr}$ . It is generally thought that the active lifetime of a fallback disk is  $\sim 10^5 \text{ yr}$  (Gençali et al. 2022), thus, the probability that J1839 is in the propeller phase can be ruled out.

#### 3.3.2. J1839 is in the second ejector phase

J1839 may experience the first ejector phase, and the propeller phase in a timescale of  $10^5 \text{ yr}$  that the fallback disk is active. Subsequently, the source transitions to the second ejector phase again because the fallback disk becomes inactive. Figure 7 shows the evolutionary tracks of  $P$  and  $\dot{P}$  of NSs with an initial mass-accretion rate  $\dot{M}_0 = 4.0 \times 10^{24} \text{ g s}^{-1}$  and different magnetic fields. The NS with a weak magnetic field of  $B = 1.0 \times 10^{13} \text{ G}$  is consistently in the ejector phase and evolves to a period of  $\sim 10 \text{ s}$  in a timescale of  $10^8 \text{ yr}$ . The NS with a strong magnetic field of  $B = 1.0 \times 10^{15} \text{ G}$  can evolve to the present period of J1839 in the quasi-spin equilibrium stage, while the corresponding period derivative is much higher than the observed value.

Only the NS with  $B = 2.0 \times 10^{14} \text{ G}$  successively experiences the first ejector phase, the propeller phase, the quasi-spin equilibrium stage, and the second ejector phase. When the NS age of  $t = 10^5 \text{ yr}$ , the NS was spun down to a period of 1200 s in the quasi-spin equilibrium stage. Subsequently, it transitions to the second ejector phase because the fallback disk becomes inactive. Because the initial period  $P_0 = 1200 \text{ s}$  in the second ejector phase, the  $t_{\text{em}}$  is approximately 10 orders of magnitude longer than that in the first phase. Since  $t \ll t_{\text{em}}$ , the period of the NS increases at an extremely small rate, which is consistent with the low  $\dot{P}$  observed in J1839. At  $t = 2.5 \times 10^7 \text{ yr}$ , the period of the NS increases to the current period (1318 s) of J1839, and the period derivative decreases to be  $\dot{P} = 8.0 \times 10^{-14} \text{ s s}^{-1}$ , which is less

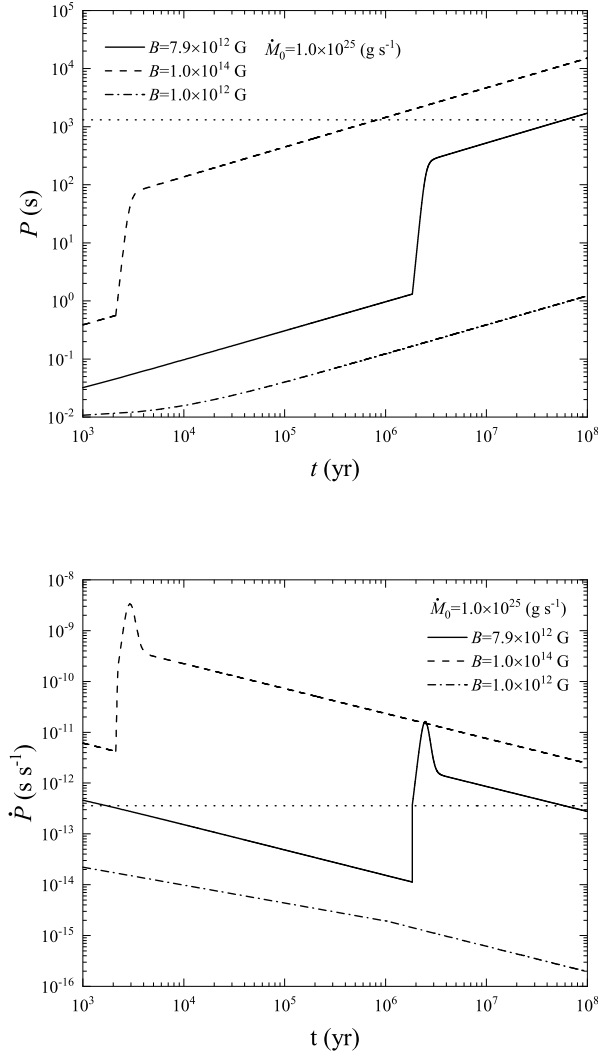


**Figure 6.** Evolution of NSs with a fallback disk of an initial mass-accretion rate  $\dot{M}_0 = 1.0 \times 10^{25}$   $\text{g s}^{-1}$  and different surface magnetic fields in the spin period vs. NS age diagram (top panel) and period derivative vs. NS age diagram (bottom panel). The fallback disks are assumed to be always active. The horizontal dotted line in the top panel and bottom panel represents the present period  $P = 1318$  s and the upper limit ( $\dot{P} = 3.6 \times 10^{-13}$   $\text{s s}^{-1}$ ) of the period derivative of radio transient J1839, respectively.

than the observed upper limit of  $\dot{P} = 3.6 \times 10^{-13}$   $\text{s s}^{-1}$ . At  $t = 10^5$  yr, the propeller torque exerted on the NS changes into the magnetic dipole radiation torque, thus, the  $\dot{P}$  sharply decreases.

To understand the influence of  $\dot{M}_0$  on the spin evolution of NSs, we also chart the evolution of the spin periods of NSs with  $B = 2.0 \times 10^{14}$  G and  $\dot{M}_0 = 4.0 \times 10^{23}$ ,  $4.0 \times 10^{24}$ , and  $4.0 \times 10^{25}$   $\text{g s}^{-1}$  in Figure 8. Since the

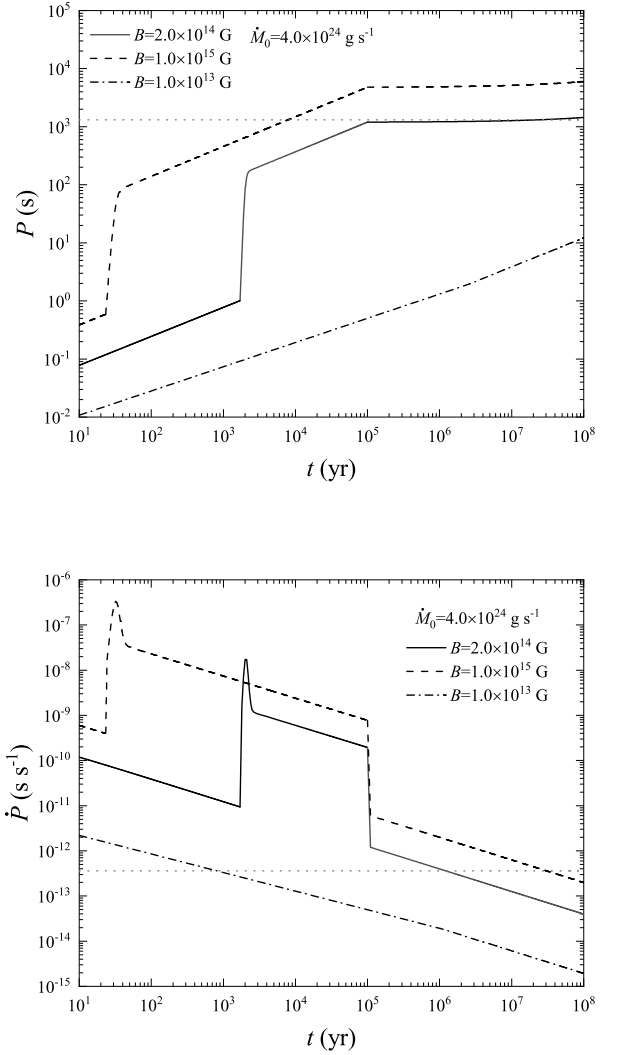


**Figure 7.** Same as Figure 6 but for  $\dot{M}_0 = 4.0 \times 10^{24}$   $\text{g s}^{-1}$  and  $B = 1.0 \times 10^{13}$ ,  $2.0 \times 10^{14}$ , and  $1.0 \times 10^{15}$  G. Furthermore, the fallback disks are thought to be inactive after the NS age is greater than  $10^5$  yr.

duration of the first ejector phase  $t_{\text{ej}} \propto \dot{M}_0^{-16/9}$ , the NS with a small initial mass-accretion rate of  $4.0 \times 10^{23}$   $\text{g s}^{-1}$  cannot transition to the propeller phase in a timescale of  $10^8$  yr. However, the NS with a high initial mass-accretion rate of  $4.0 \times 10^{25}$   $\text{g s}^{-1}$  enters the propeller phase in a short timescale of  $\sim 30$  yr.

To investigate the progenitor properties of J1839, in Figure 9 we summarize the parameter space that can produce the ultra-long period radio transient J1839 in magnetic field versus the initial mass-accretion rate diagram. The characteristic age of J1839 is  $\tau_c = P/(2\dot{P}) > 1.2 \times 10^8$  yr. In the simulation, we diagnose whether an NS can evolve to the current state of J1839 in a timescale

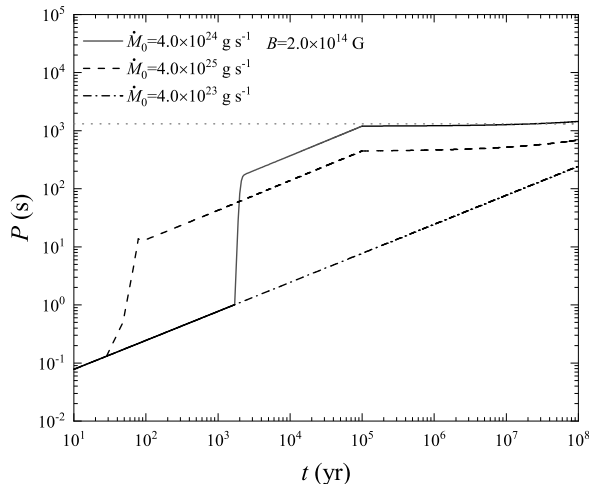


**Figure 8.** Same as the top panel of Figure 7 but for  $B = 2.0 \times 10^{14}$  G and  $\dot{M}_0 = 4.0 \times 10^{23}, 4.0 \times 10^{24}$ , and  $4.0 \times 10^{25}$  g s $^{-1}$ .

of  $1.2 \times 10^8$  yr. It is clear that the potential progenitor of J1839 is also a magnetar. Those magnetars with a magnetic field of  $(2 - 6) \times 10^{14}$  G and a fallback disk with an initial mass-accretion rate of  $4.0 \times 10^{24} - 10^{26}$  g s $^{-1}$  are possible progenitors of radio transient J1627. Similar to J1627, a strong magnetic field tends to require a high initial mass-accretion rate in order to evolve into J1839. Furthermore, an NS with a magnetic field stronger than  $6.0 \times 10^{14}$  G can evolve to the observed period of J1839, while the corresponding period derivative is much higher than the observed value.

#### 4. DISCUSSION

##### 4.1. Comparison with previous works

Assuming an initial spin period  $P_0 = 10$  ms and an initial mass-accretion rate  $\dot{M}_0 \sim 10^{23}$  g s $^{-1}$ , Ronchi et al. (2022) found that a magnetar with initial magnetic field  $B_0 \sim 10^{14}$  G can spin down to a spin period of 1091 s in a timescale of  $10^3 - 10^5$  yr. However, our models require a relatively high initial mass-accretion rate of  $\gtrsim 10^{24}$  g s $^{-1}$ . This discrepancy should arise from their different accretion model of the fallback disk, in which  $\dot{M} = \dot{M}_0(1 + t/T)^{-\alpha}$  (Menou et al. 2001; Ertan et al. 2009). Furthermore, they considered the decay of magnetic fields under the combined contribution of ohmic dissipation and the Hall effect in the NS crust, which causes the NS to slightly spin up after the spin equilibrium. However, our simulated spin period slowly increases during the quasi-spin equilibrium.

Adopting a same model in Tong et al. (2016), Tong (2023a) found that a magnetar with a magnetic field

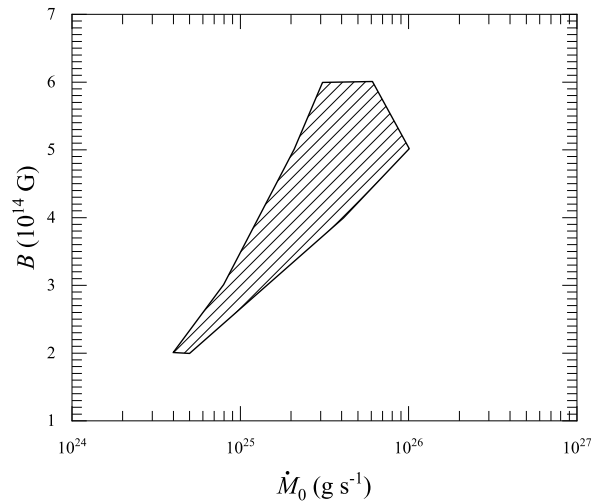


**Figure 9.** Parameter space that can produce the ultra-long period radio transient J1839 in magnetic field vs. initial mass-accretion rate diagram. Those nascent NSs with a magnetic field and an initial mass-accretion rate in the shaded region can evolve into the radio transient J1839 with a spin period of 1318 s and a period derivative less than  $3.6 \times 10^{-13}$  s s $^{-1}$  in a timescale shorter than  $1.2 \times 10^8$  yr. The fallback disks are assumed to be inactive after the NS age is greater than  $10^5$  yr.

$B = 4.0 \times 10^{14}$  G can be spun down to 1091s by a self-similar fallback disk with initial mass of  $M_{d,i} = 10^{-3} - 10^{-4} M_\odot$ . From  $\dot{M}_0 = (\alpha - 1)M_{d,i}/(\alpha T)$ , the corresponding initial mass-accretion rates are  $1.6 \times (10^{25} - 10^{26})$  g s $^{-1}$ . According to our simulated parameter space forming J1627, an NS with  $\dot{M}_0 = 1.6 \times 10^{25}$  g s $^{-1}$  and  $B = 4.0 \times 10^{14}$  G can evolve into J1627, while an NS with  $\dot{M}_0 = 1.6 \times 10^{26}$  g s $^{-1}$  and  $B = 4.0 \times 10^{14}$  G is unlikely to evolve toward J1627 in a timescale less than  $10^5$  yr. This discrepancy may be caused by different determining criterion forming J1627, in which the spin period is a unique criterion in Tong (2023a), while both  $P$  and  $\dot{P}$  are criterions forming J1627 in our simulations.

Gençali et al. (2022) shown that an NS with an initial period of 0.3 s, a magnetic field of  $\sim 10^{12}$  G, and a fallback disk with an initial mass of  $1.6 \times 10^{-5} M_\odot$  can evolve into J1627. Their simulations can interpret the observed period, period derivative, and X-ray luminosity of J1627 when the disk becomes completely inactive in a timescale of  $7 \times 10^5$  yr. Our magnetic field is much stronger than that in their model, and the evolutionary timescale is one order of magnitude smaller than their result. Different torque models should be responsible for these discrepancies.

#### 4.2. Evolutionary fates of NSs under different input parameters

According to the NS + fallback disk model, the evolutionary fates of pulsars depend on the two input parameters: magnetic field  $B$  and initial mass-accretion rate  $\dot{M}_0$  of the fallback disk. In the  $\dot{P} - P$  diagram of pulsars, we depict the evolutionary tracks of NSs with several special  $B$  and  $\dot{M}_0$ . An NS with a weak magnetic field of  $2.0 \times 10^{13}$  G is always in the ejector phase and evolves into a normal pulsar. The two NSs with  $B = 2.0 \times 10^{14}$  G, and  $\dot{M}_0 = 1.5 \times 10^{24}$  and  $4.0 \times 10^{24}$   $\text{g s}^{-1}$  evolve toward radio transients with an ultra-long period and a relatively high  $\dot{P} \sim 10^{-10} - 10^{-9} \text{ s s}^{-1}$  in the propeller phase. Such a  $\dot{P}$  is compatible with the observed upper limit of J1627, hence J1627 is probably in the propeller phase. However, J1839 has a very small period derivative as  $\dot{P} < 3.6 \times 10^{-13} \text{ s s}^{-1}$ . Therefore, the evolutionary state of J1839 should be different with J1627. Assuming a fallback-disk active timescale of  $10^5$  yr, our models show that the magnetic dipole torque in the second ejector phase can produce a  $\dot{P}$  that is compatible with the observed upper limit of J1839.

J0901 is a long period pulsar with a period of  $P = 75.9$  s and a period derivative of  $\dot{P} = 2.25 \times 10^{-13} \text{ s s}^{-1}$  (Caleb et al. 2022). If this NS is spinning down by a pure magnetic dipolar radiation, the dipolar magnetic field can be estimated to be  $B = 1.3 \times 10^{14}$  G (Ronchi et al. 2022). Our simulations indicate that an NS with a strong magnetic field of  $B = 1.0 \times 10^{14}$  G and a high initial mass-accretion rate of  $\dot{M}_0 = 1.0 \times 10^{27} \text{ g s}^{-1}$  can evolve to the current state of J0901 in the second ejector phase. Recently, Gençali et al. (2023) found that an NS with a weak magnetic field of  $\sim 10^{12}$  G can evolve to the current state of J0901 in the strong propeller phase.

J0250 is another slow-spinning radio pulsar with a spin period of 23.5 s and a spin-period derivative of  $\dot{P} = 2.7 \times 10^{-14} \text{ s s}^{-1}$  (Tan et al. 2018). In Figure 10, the observed  $P$  and  $\dot{P}$  of J0250 can be matched by the blue evolutionary track, in which the nascent NS has a magnetic field of  $B = 4.0 \times 10^{13}$  G and  $\dot{M}_0 = 2.0 \times 10^{28} \text{ g s}^{-1}$ . The required magnetic field in our model is approximately equal to the inferred one ( $B = 2.6 \times 10^{13}$  G, Tan et al. 2018). To evolve into the current states of J0901 and J0250, it requires extremely high initial mass-accretion rates of  $10^{27} - 10^{28} \text{ g s}^{-1}$ . According to Equation (9), the duration of the first ejector phase  $t_{\text{ej}} \propto \dot{M}^{-4/7}$ , thus, these two sources merely experience a very short timescale in the first ejector.

#### 4.3. Influence of magnetic field decay

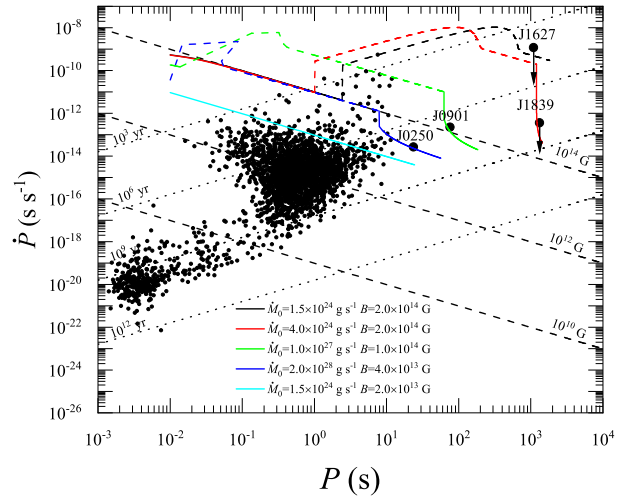


**Figure 10.** Evolutionary fates of NSs with different  $B$  and  $\dot{M}_0$  in the  $\dot{P} - P$  diagram. The solid and dashed curves represent the evolutionary tracks in the ejector phase and the propeller phase, respectively. The arrows of J1627 and J1839 stand for their possible range of  $\dot{P}$ . The fallback disks are assumed to be inactive after the NSs ages are greater than  $10^5$  yr.

In the calculations, we ignore a decay of the magnetic field. Actually, the magnetic fields of NSs ought to decay due to the ohmic dissipation and the Hall effect in their crusts (Pons & Geppert 2007; Pons et al. 2009; Viganò et al. 2013; Pons & Viganò 2019; De Grandis et al. 2020). An evolution simulation shown that the decay of an initial magnetic field of  $10^{14}$  G cannot influence the spin-period evolution of the ejector phase in a timescale of  $10^4$  yr (see also Figure 1 of Ronchi et al. 2022). However, the decay of magnetic fields would produce a long  $t_{\text{prop}}$  according to Equation (14). As a consequence, J1627 would take a relatively long timescale to evolve to the current period.

If J1839 can evolve to an ultra-long period that is very close to the current period in the active stage of the fallback disk, it would naturally transition to the second ejector phase. Since  $t_{\text{em}} \propto B^{-2}$  according to Equation (7), a decaying magnetic field leads to a relatively long  $t_{\text{em}}$ . Therefore, the increase of the period is slower than the case without magnetic field decay. Accordingly, the evolutionary timescale of J1839 is also slightly longer than our calculation.

## 5. CONCLUSIONS

Recently, a radio transient J1627 with an unusually ultra-long period of 1091 s was reported, and it was proposed to be an ultra-long-period magnetar (Hurley-Walker et al. 2022). In this work, we attempt

to diagnose whether a magnetar with a fallback disk could be spun down to the current spin period of J1627 by the propeller torque. Our simulations indicate that an NS with a magnetic field of  $B = (2 - 5) \times 10^{14}$  G and a fallback disk with an initial mass-accretion rate of  $\dot{M}_0 = (1.1 - 30) \times 10^{24} \text{ g s}^{-1}$  can evolve into J1627 in a timescale less than  $10^5$  yr. The models with magnetar + fallback disk can account for the spin period, period derivative, and X-ray luminosity of J1627.

Because of a small upper limit of the period derivative, the origin of another radio transient J1839 remains mysterious. Our simulations show that the NS + fallback disk model can account for the observed period and period derivative of J1839, while the required timescale is  $\sim 10^7$  yr, which is much longer than the possible active timescale ( $\sim 10^5$  yr) of a fallback disk. Therefore, we propose that J1839 may be in the inactive stage of a fallback disk similar to Gençali et al. (2022). Taking an active timescale of  $10^5$  yr, the propeller torque of the fallback disk exerted on an NS can spin it down to a period of 1200 s in the quasi-spin-equilibrium stage. After the fallback disk becomes inactive, the NS can evolve to the current period and period derivative of J1839 in the second ejector phase. Those NSs with a magnetic field of  $B = (2 - 6) \times 10^{14}$  G and a fallback disk with an initial mass-accretion rate of  $\dot{M}_0 \sim 10^{24} - 10^{26} \text{ g s}^{-1}$  are

the possible progenitors of J1839, which can evolve into J1839 in a timescale less than its characteristic age.

Our simulations also show that the evolutionary fates of NSs in the  $\dot{P} - P$  diagram are very sensitive to the two input parameters including  $B$  and  $\dot{M}_0$ . The NS with a weak magnetic field or a low mass-accretion rate naturally evolves toward a normal pulsar. The strong magnetic field NS + fallback disk model can interpret two ultra-long period radio transients and those long-period pulsars. It is worth emphasizing that ultra-long period radio transient J1627 with a high  $\dot{P}$  ought to be in the quasi-spin equilibrium stage, while the transient J1839 and two long-period pulsars evolve to the second ejector phase at present. Certainly, there are many uncertainties in the nature of J1839. A relatively accurate  $\dot{P}$  may provide a reliable constraint whether or not it is a radio magnetar. More multiwave observations can also help us to unveil the mysterious nature of J1839.

#### ACKNOWLEDGMENTS

We are extremely grateful to the anonymous referee for helpful comments that improved this manuscript. We thank H. Tong, and K. Qin for helpful discussions. This work was partly supported by the National Natural Science Foundation of China (under grant Nos. 12273014 and 12203051), and the Natural Science Foundation (under grant No. ZR2021MA013) of Shandong Province.

#### REFERENCES

- Beniamini, P., Wadiasingh, Z., Hare, J. et al. 2023, MNRAS, 520, 1872
- Beniamini, P., Wadiasingh, Z., & Metzger, B. D. 2020, MNRAS, 496, 3390
- Bhattacharya, D., & van den Heuvel, E. P. J. 1991, PhR, 203, 1
- Borghese, A., Coti Zelati, F., Esposito, P., et al. 2018, MNRAS, 478, 741
- Braun, C., Safi-Harb, S., Fryer, C. L. 2019, MNRAS, 489, 4444
- Caleb, M., Heywood, I., Rajwade, K., et al. 2022, NatAs, 6, 828
- Cannizzo, J. K., Lee, H. M., & Goodman, J. 1990, ApJ, 351, 38
- Carter, L. M., Dickel, J. R., & Bomans, D. J. 1997, PASP, 109, 990
- Chatterjee, P., Hernquist, L., & Narayan, R. 2000, ApJ, 534, 373
- Chen, K., & Ruderman, M. 1993, ApJ, 402, 264
- Chen, W.-C. 2022, A&A, 662, A79
- Clark, D. H., & Caswell, J. L. 1976, MNRAS, 174, 267
- Cui, W. 1997, ApJL, 482, L163
- Daumerie, P. R. 1996, Ph.D. thesis, Univ. Illinois
- D’Ài, A., Evans, P. A., Burrows, D. N., et al., 2016, MNRAS, 463, 2394
- Davidson, K., & Ostriker, J. P. 1973, ApJ, 179, 585
- De Grandis, D., Turolla, R., Wood, T. S., et al. 2020, ApJ, 903, 40
- De Luca, A., Caraveo, P. A., Mereghetti, S., Tiengo, A., & Bignami, G. F. 2006, Science, 313, 814
- De Luca, A., Mignani, R. P., Zaggia, S., Beccari, G., Mereghetti, S., Caraveo, P. A., & Bignami, G. F. 2008, ApJ, 682, 1185
- Elsner, R. F., & Lamb, F. K. 1977, ApJ, 215, 897
- Erkut, M. H. 2022, MNRAS, 514, L41
- Ertan, Ü., Ekşi, K. Y., Erkut, M. H., & Alpar, M. A. 2009, ApJ, 702, 1309
- Esposito, P., Turolla, R., de Luca A. et al. 2011, MNRAS, 418, 170
- Gençali, A. A., Ertan, Ü., & Alpar, M. A. 2022, 513, L68

- Gençali, A. A., Ertan, Ü., & Alpar, M. A. 2023, 520, L11
- Gold, T. 1968, *Nature*, 218, 731
- Ghosh, P., & Lamb, F. K. 1979, *ApJ*, 232, 259
- Han, J. L., Wang, C., Wang, P. F., et al. 2021, *RAA*, 21, 107
- Hewish, A., Bell, S. J., Pilkington, J. D., Scott, P. F., & Collins, R. A. 1968, *Nature*, 217, 709
- Ho, W. C. G., & Andersson, N. 2017, *MNRAS*, 464, L65
- Hurley-Walker, N., Rea, N., McSweeney, S. J., et al. 2023, *Nature*, 619, 487
- Hurley-Walker, N., Zhang, X., Bahramian, A. et al. 2022, *Nature*, 601, 526
- Illarionov, A. F., & Sunyaev, R. A. 1975, *A&A*, 39, 185
- Kaplan, D. L., Chakrabarty, D., Wang, Z., & Wachter, S. 2009, *ApJ*, 700, 149
- Katz, J. I. 2022, *Ap&SS*, 367, 108
- Kou, F. F., Tong, H., Xu, R. X., & Zhou, X. 2019, *ApJ*, 876, 131
- Levin, L., Bailes, M., Bates, S. D., et al. 2012, *MNRAS*, 422, 2489
- Li, X.-D. 2006, *ApJL*, 646, L139
- Li, X.-D. 2007, *ApJL*, 666, L81
- Lin, D. N. C., Woosley, S. E., & Bodenheimer, P. H. 1991, *Nature*, 353, 827
- Loeb, A., & Maoz, D. 2022, *RNAAS*, 6, 27
- Long, M., Romanova, M. M., & Lovelace, R. V. E. 2005, *ApJ*, 634, 1214
- Manchester, R. N., Hobbs, G. B., Teoh, A., & Hobbs, M. 2005, *AJ*, 129, 1993
- Menou, K., Esin, A. A., Narayan, R. et al. 1999, *ApJ*, 520, 276
- Menou, K., Perna, R., & Hernquist, L. 2001, *ApJ*, 559, 1032
- Michel, F. C. 1988, *Nature*, 333, 644
- Nugent, J. J., Pravdo, S. H., Garmire, G. P., Becker, R. H., Tuohy, I. R., & Winkler, P. F. 1984, *ApJ*, 284, 612
- Olausen, S. A., & Kaspi, V. M. 2014, *ApJS*, 212, 6
- Papitto, A., & Torres, D. F. 2015, *ApJ*, 807, 33
- Pons, J. A., & Geppert, U. 2007, *A&A*, 470, 303
- Pons, J. A., Miralles, J. A., & Geppert, U. 2009, *A&A*, 496, 207
- Pons, J. A., & Viganò, D. 2019, *LRCA*, 5, 3
- Tsygankov, S. S., Mushtukov, A. A., Suleimanov, V. F., & Poutanen, J. 2016, *MNRAS*, 457, 1101
- Perna, R., Duffell, P., Cantiello, M., & MacFayden, A. I. 2014, *ApJ*, 781, 119
- Rea, N., Borghese, A., Esposito, P., Coti Zelati, F., Bachetti, M., Israel, G. L., & De Luca A. 2016, *ApJ*, 828, L13
- Ronchi, M., Rea, N., Graber, V., & Hurley-Walker, N. 2022, *ApJ*, 934, 184
- Ruderman, M. A., & Sutherland, P. G. 1975, *ApJ*, 196, 51
- Tan, C. M., Bassa, C. G., Cooper, S., et al. 2018, *ApJ*, 866, 54
- Tauris, T. M., & van den Heuvel, E. P. J. 2006, in *Formation and Evolution of Compact Stellar X-ray Sources*, ed. W. H. G. Lewin & M. van der Klis (Cambridge: Cambridge Univ. Press), 623
- Tendulkar, S. P., Kaspi, V. M., Archibald, R. F., & Scholz, P. 2017, *ApJ*, 841, 11
- Tong, H. 2023a, *ApJ*, 943, 3
- Tong, H. 2023b, *RAA*, 23, 125018
- Tong, H., Wang, W., Liu, X. W., & Xu, R. X. 2016, *ApJ*, 833, 265
- Viganò, D., Rea, N., Pons, J. A., et al. 2013, *MNRAS*, 434, 123
- Wang, Y.-M. 1996, *ApJ*, 465, L111
- Wang, Z., Chakrabarty, D., & Kaplan, D. L. 2006, *Natur*, 440, 772
- Xu, K., & Li, X.-D. 2019, *ApJ*, 877, 138
- Zhang, S. N., Yu, W., & Zhang, W. 1998, *ApJL*, 494, L71